





Article

Magnesium Oxychloride Cement Composites Lightened with Granulated Scrap Tires and Expanded Glass

Milena Pavlíková ¹, Adam Pivák ¹, Martina Záleská ¹, Ondřej Jankovský ², Pavel Reiterman ³ and Zbyšek Pavlík ^{1,*}

- ¹ Department of Materials Engineering and Chemistry, Faculty of Civil Engineering, Czech Technical University in Prague, Thákurova 7, 166 29 Prague 6, Czech Republic; milena.pavlikova@fsv.cvut.cz (M.P.); adam.pivak@fsv.cvut.cz (A.P.); martina.zaleska@fsv.cvut.cz (M.Z.)
- ² Department of Inorganic Chemistry, Faculty of Chemical Technology, University of Chemistry and Technology, Technická 5, 166 28 Prague 6, Czech Republic; ondrej.jankovsky@vscht.cz
- ³ Experimental Centre, Faculty of Civil Engineering, Czech Technical University in Prague, Thákurova 7, 166 29 Prague 6, Czech Republic; pavel.reiterman@fsv.cvut.cz
- * Correspondence: pavlikz@fsv.cvut.cz; Tel.: +42-0-224-354-371

Received: 29 September 2020; Accepted: 27 October 2020; Published: 28 October 2020



Abstract: In this paper, light burned magnesia dispersed in the magnesium chloride solution was used for the manufacturing of magnesium oxychloride cement-based composites which were lightened by granulated scrap tires and expanded glass. In a reference composite, silica sand was used only as filler. In the lightened materials, granulated shredded tires were used as 100%, 90%, 80%, and 70% silica sand volumetric replacement. The rest was compensated by the addition of expanded glass granules. The filling materials were characterized by particle size distribution, specific density, dry powder density, and thermal properties that were analyzed for both loose and compacted aggregates. For the hardened air-cured samples, macrostructural parameters, mechanical properties, and hygric and thermal parameters were investigated. Specific attention was paid to the penetration of water and water-damage, which were considered as crucial durability parameters. Therefore, the compressive strength of samples retained after immersion for 24 h in water was tested and the water resistance coefficient was assessed. The use of processed waste rubber and expanded glass granulate enabled the development of lightweight materials with sufficient mechanical strength and stiffness, low permeability for water, enhanced thermal insulation properties, and durability in contact with water. These properties make the produced composites an interesting alternative to Portland cement-based materials. Moreover, the use of low-carbon binder and waste tires can be considered as an eco-efficient added value of these products which could improve the environmental impact of the construction industry.

Keywords: magnesium oxychloride cement; scrap tires; granulated expanded glass; macrostructural parameters; mechanical resistance; thermal performance; water resistance

1. Introduction

The management, treatment, and disposal of solid waste belong among the main environmental concerns around the globe. With respect to sustainability, the best solutions of waste management are those that minimize the environmental impact at an affordable cost [1,2]. Today, the increasing population leads to an increasing number of vehicles and massive tire production. Consequently, this generates a significant increment in solid waste and, thus, in the volume of scrap tires. Therefore,

the sustainable management of end-of-life tires (ELTs) is of the particular importance. According to the ETRMA (European Tyre and Rubber Manufacturers' Association), the tire production within EU countries remained over 4 billion tons throughout the period 2010–2018 and reached a maximum of 5.1 billion tons in 2017 and 2018 [3]. This corresponds to approx. 24% of the total world production. It is estimated that EU countries, USA, Japan, India, and China produce almost 88% of the total number of withdrawn tires around the globe [4].

In Europe, most of the ELTs are recovered as reported in statistics by ETRMA [3]. In 2010, 96% of ELTs were recovered in energy (38%), materials recycling and reuse (40%), reconstruction (8%), and export (10%) [5]. On the other hand, the remaining 0.2 billion tones represents an open field for other commercial reuse of materials based on scrap tires. Moreover, in less-developed countries, the recovery of ELTs is much lower [6]. This opens a broad field for an alternative recycling of scrap tires as their stockpiling has become unacceptable because of the depletion of available sites for landfilling and fire hazards. Basically, ELTs can be managed in a number of forms, such as whole tire, slit tire, shredded or chopped tire, powdered tire, ground rubber, or as a crumb rubber product. In this respect, intensive research has been conducted to find novel and effective methods of ELT treatment. Except the use of scrap tires for energy recovery (tire-derived fuel) and alternative fuel for cement clinker production, where embodied steel sufficiently endows raw flour by iron oxides [7], they have found application in the production of building materials, such as asphalt pavements [8–11], rubberized asphalt [12,13], rubber-filled concrete [14–19], crumb rubber concrete hollow blocks [20], thermal and sound insulation precast concrete panels [21], and rendering mortars with increased durability and thermal insulation performance [22]. As tire-recycling products have low gravity, low thermal conductivity, and are waterproof and durable against harmful environmental action, they have found use in the construction of tunnels, underground passages, highway embankments, acoustic sheets, acoustic flooring foils, etc. [4]. The rubber from worn tires were also found to improve the resistance of cement mortars against water and chloride penetration [23,24]. Recently, rubber particles were found to have potential to be used as bacteria carriers in self-healing concrete [25].

Typically, the high dosage of rubber in concrete led to an excessive drop in mechanical resistance due to the failure of the bond between rubber particles and the silicate matrix, and a reduction in bulk density and elastic modulus. However, processed tires can find use in other types of composites and construction products, where high mechanical strength is not the main technical parameter. For example, they can be applied in the form of lightweight fillers or admixtures providing low permeability for water and dissolved salt, thus ensuring durability in terms of water resistance, ability to absorb deformation without cracking, improved freeze/thaw resistance [26], etc.

As the use of ELTs in Portland cement- and asphalt-based materials was intensively explored within last three decades, we aimed in the presented work at the use of granulated waste tire rubber as lightweight water resistant aggregate in composition of composites made of magnesium oxychloride cement (MOC) as an only binder. The impact of the use of rubber granulate on the technical and functional properties and performance of the researched materials was studied and the findings are discussed and summarized. The research was motivated by the fact the Portland cement industry has an adverse environmental impact which is associated with enormous CO₂ emissions and natural resources depletion. MOC has many superior properties to those associated with ordinary Portland cement, such as fast hardening, early and high strength, low alkalinity, low density of precipitated products, fire resistance, high bonding ability, CO₂-neutrality, etc. [27–29]. On the other hand, a critical defect of MOC is its limited water resistance which is the cause of its little industrial application [30,31]. As the rubber produced from scrap tires repels water (hydrophobic nature), it is assumed it will restrict water transport in the MOC matrix and, thus, ensure its resistance with regard to water damage. It is also expected that the lightweight rubber will help to enhance thermal insulation performance of the final composites. Similar benefits should also be provided by granulated expanded glass, which was used in composite mixtures as a partial substitute of processed waste tires. The motivation of the paper can be summarized as: the design, development, and testing of lightweight eco-efficient MOC

composites with improved water resistance and thermal insulation capability. The novelty of the presented study is evident as the use of recycled waste tires in MOC composites was only rarely studied up to now, and data on hygric and thermo-physical properties of MOC/granulated rubber composites are not available at all.

2. Materials and Methods

For preparation of MOC binder, $\text{MgCl}_2 \cdot 6\text{H}_2\text{O}$ (purity > 99%, Lach-Ner, s.r.o., Neratovice, Czech Republic) and MgO produced by Styromagnesit Steirische Magnesitindustrie Ltd. (Oberdorf, Austria) were used. The chemical composition of caustic MgO was following: MgO_2 (81.5 wt%), SiO_2 (3.6 wt%), Al_2O_3 (5.5 wt%), CaO (4.7 wt%), Fe_2O_3 (4.0 wt%), SO_3 (0.6 wt%).

In the reference composite (MOC-S) silica sand, a particle size in the range of 0–2 mm was dosed as the only filler. It was delivered by Filtrační písky, spol. s.r.o. (Chlum u Doks, Czech Republic). Silica sand was used as a mixture of three sand fractions (0.063–0.5 mm, 0.5–1.0 mm, 1.0–2.0 mm) which were mixed in a mass ratio 1:1:1. The main constituents of sand were SiO_2 (97.1 wt%), Al_2O_3 (2.3 wt%), MgO (0.3 wt%), and TiO_2 (0.2 wt%). The chemical composition of silica sand and MgO was measured using an ED-XRF spectrometer ARL QUANT'X (Thermo Fisher Scientific, Waltham, MA, USA). For data collection and analysis, UniQuant 5 software (Thermo Scientific, Milan, Italy) was applied.

The rubber granulate was produced by Montstav CZ s.r.o. (Dolní Rychnov, Czech Republic) by mechanical processing of waste tires, which is the most frequently used technology for rubber reclaiming [32]. The recycling of ELTs starts with the pulling out of the heel rope, which would cause an excessive wear of the crusher cutting tool. Thereafter, the tire is transported to the knife mill hopper by using a conveyor belt. The mill grinds the tire to so-called “chips” of different dimensions, which are subsequently sorted out in accordance with the actual requirements; the largest pieces returning to the mill. The process of secondary mechanical crushing is carried out in a different device which has the specified design of the crushing knives. Originating grit continues through a magnetic sorter to omit steel fibers. Resulting rubber grit is sorted to the various grades. In our case, the maximum size of rubber granulate was 2 mm (mix of fractions 0–1 mm, 1–2 mm). The processing of waste tires by Montstav CZ s.r.o. is shown in Figure 1.

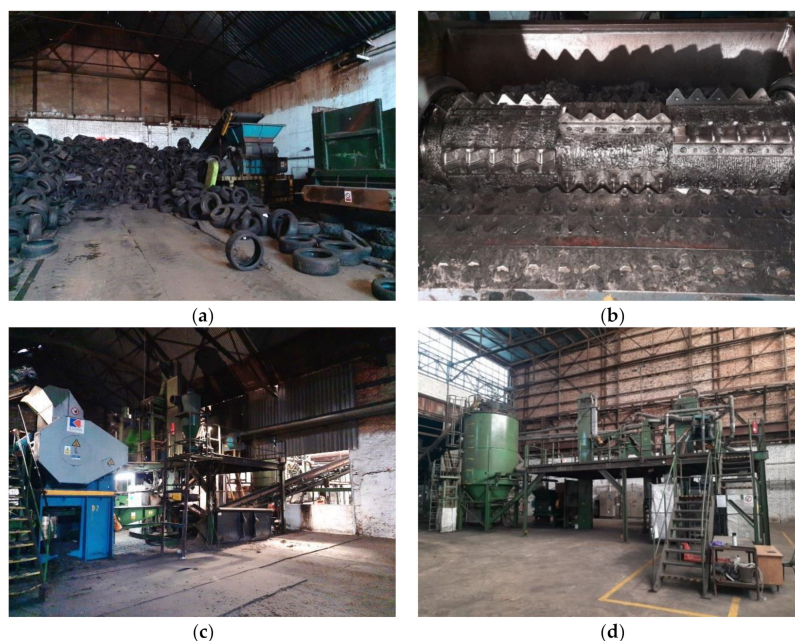


Figure 1. The mechanical processing of waste tires, (a) tires' stocking and transportation, (b) knife mill, (c) sorting of rubber chips, (d) secondary crushing.

Expanded glass granulate, commercial name Liaver (Liaver GmbH and Co. KG, Ilmenau, Germany) is produced from recycled glass and sintered at temperatures from 750 °C to 900 °C in a rotary kiln. It is composed of SiO₂ (71 ± 2 wt%), Al₂O₃ (2 ± 0.3 wt%), Na₂O (13 ± 1 wt%), Fe₂O₃ (0.5 ± 0.2 wt%), CaO (8 ± 2 wt%), MgO (2 ± 1 wt%), K₂O (1 ± 0.2 wt%). The data was taken from the technical sheet of the product). In our case, we mixed four Liaver fractions originally manufactured to obtain similar particle size distribution as that of silica sand. The wt% of particular Liaver fractions were as follows: 0.1–0.3 mm 23%, 0.25–0.5 mm 22%, 0.5–1 mm 25%, 1–2 mm 30%. Both alternative lightweight fillers, i.e., shredded rubber and expanded glass granulate, are shown in Figure 2. In the case of granulated rubber, particles and plates of different size, thickness, and shape were observed. The particles of glass granulate were oval- and sphere-shaped, and their size corresponded with the measured particle size curve.

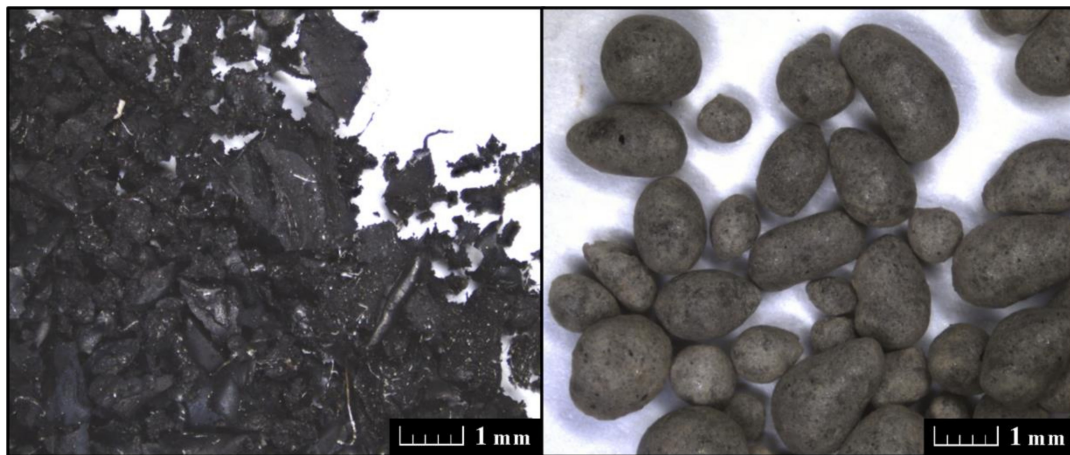


Figure 2. Rubber granulate (**left**) and expanded glass granulate (**right**), scale bar: 1 mm.

Silica sand, granulated rubber, and Liaver were characterized by specific density ρ_{sf} (kg·m⁻³) that was measured using a Pycnomatic ATC helium pycnometer (Porotec, Hofheim, Germany). For applied fillers, powder density ρ_p (kg·m⁻³) and thermal parameters were measured in loose and compacted states. The compaction was conducted with a vibration exciter for 90 s. The powder density was determined by the use of graduated cylinder (sample volume), and precise laboratory scales (sample mass) A&D GX 20,021 (A&D weighing, Adelaide, Australia). The measurement of fillers thermal conductivity λ_f (W·m⁻¹·K⁻¹) and volumetric heat capacity C_{vf} (J·m⁻³·K⁻¹) was performed with an Isomet 2114 apparatus (Applied Precision, Bratislava, Slovakia) equipped with a needle probe for measurement of granular and powdered substances. The apparatus operates on a nonstationary heat impulse technique [33] with the accuracy 5% of reading + 0.001 W·m⁻¹·K⁻¹ for λ in the range of 0.015–0.70 W·m⁻¹·K⁻¹, and 10% of the reading for λ ranging from 0.70 W·m⁻¹·K⁻¹ to 6.0 W·m⁻¹·K⁻¹. The volumetric heat capacity was obtained with accuracy 15% of reading + 1 × 10³ J·m⁻³·K⁻¹. The grain size analysis was also conducted by standard sieve method as prescribed in EN 933-1 [34]. The used sieves had mesh dimension 0.063, 0.125, 0.25, 0.5, 1.0, and 2.0 mm, respectively.

Rubber granulate was used as a full (material labelled MOC-WT) and partial silica sand replacement. The replacement ratio was 90%, 80%, and 70% by volume. In composites, where silica sand was only partially substituted, the rest of filler volume was supplemented with Liaver. These composites were marked MOC-WT+L10, MOC-WT+L20, and MOC-WT+L30, respectively. The composition of the investigated MOC-based composites is introduced in Table 1. These were mixed and prepared in accordance with the EN 14016-2 [35] that defines dosage of MgO, MgCl₂, and water for preparation of pastes based on MgO of p.a. purity. Therefore, the dosage of MgO in composite mixtures was higher in order to ensure the precipitation of MOC phases. We used a similar approach in our recently published paper [36], where the design and testing of MOC composites with coal fly ash admixture was presented.

Table 1. The weight proportioning of designed composites (g), the dosage of MgO, MgCl₂·6H₂O, and water was kept constant for all produced mixtures, and was 1350 g, 597.9 g, and 496.8, respectively.

Composite	Silica Sand	Rubber Granulate	Liaver
MOC-S	3 × 1080	-	-
MOC-WT	-	3 × 350	-
MOC-WT+L10	-	3 × 315	72.4
MOC-WT+L20	-	3 × 279.9	144.9
MOC-WT+L30	-	3 × 244.9	217.3

The water/binder ratio was 0.26 and was kept similar for all composite mixtures.

The fresh composite mixtures were casted into plastic molds that were oiled with mineral oil. The samples were prisms having dimensions 40 mm × 40 mm × 160 mm. After 24 h the samples were unmolded and left to freely cure for 13 days in laboratory at $T = (23 \pm 2) ^\circ\text{C}$, $RH = (50 \pm 5) \%$.

The testing methods were chosen in order to get complex information on the impact of the use of rubber and expanded glass granulates on technical, functional, and performance parameters of the developed composites and to characterize their resistance against harmful water action.

For fresh composite mixtures, workability was tested using a flow table test.

The hardened composites were characterized by the measurement of their macrostructural parameters, mechanical parameters, hygric, and thermal properties. The durability of the examined materials with respect to possible moisture damage was also the subject of the research. This broad experimental campaign was designed and conducted in such a way to get detailed knowledge of the properties of the developed composites which should help to assess their application potential. Bulk density, specific density, and total open porosity were the investigated macrostructural parameters. Before the particular tests, samples were dried at 30 °C in a vacuum dryer Vacucell (BMT, Brno, Czech Republic). The dry bulk density ρ_b (kg·m⁻³) was tested in accordance with the EN 1015-10 [37]. The expanded combined uncertainty of the bulk density assessment was 1.4%. The specific density ρ_s (kg·m⁻³) was measured on a helium pycnometry principle similarly as in testing of fillers (see above). The expanded combined uncertainty of this test was 1.2%. For the measurement, the fragments of samples used for strength tests were used. The typical sample mass was 2.5–3.5 g. The total open porosity Ψ (%) was calculated as:

$$\Psi = \left(1 - \frac{\rho_b}{\rho_s}\right) \cdot 100 \quad (1)$$

with the expanded combined uncertainty 2.0%.

Flexural strength f_f (MPa) was determined in a three point bending test arrangement on original casted prisms. The compressive strength f_c (MPa) was measured on the specimen fragments from flexural strength testing. The loading area was 40 mm × 40 mm. The strength tests were realized in accordance with the EN 1015-11 [38]. The expanded combined uncertainty of both strength tests was 1.4%. The stiffness of researched composites was characterized by dynamic elastic modulus E_d (GPa). It was measured using an ultrasonic data logger Vikasonic (Schleibinger Geräte, Buchbach, Germany) with the uncertainty of 2.3%. During the test, the dry casted prisms were placed between ultrasonic transducers (transmitter and receiver, 54 kHz) and the velocity of ultrasonic pulse v (m/s) travelled in the sample was obtained based on sample length l_s (m) and transmission time t_t (s). The experimental setup of the ultrasonic test is apparent from Figure 3. Based on the measured ultrasonic pulse velocity v , the dynamic elastic modulus was determined as defined in Equation (2) [39]:

$$E_d = \rho_b \left(\frac{l_s}{t_t}\right)^2 = \rho_b v^2. \quad (2)$$



Figure 3. Measurement of the dynamic elastic modulus.

As MOC is an aerial binder, MOC-based products usually deteriorate in contact with water due to the decomposition of precipitated products of binder hardening [40–42]. Therefore, the hygric properties of the developed materials were of particular importance in the presented experimental campaign. As basic hygric performance characteristic describing the water imbibition in porous media, the 24 h water absorption W_a (%) was measured following the procedure specified in the EN 13755 [43]. The expanded combined uncertainty of the assessment of parameter W_a was 1.2%. In the capillary absorption test, water absorption coefficient A_w ($\text{kg}\cdot\text{m}^{-2}\cdot\text{s}^{-1/2}$) was measured [44]. The samples had dimensions of 40 mm \times 40 mm \times 70 mm, and their lateral sides were coated with epoxy resin in order to ensure 1-D water transport. The water in reservoir stayed 3–5 mm above the sample bottom as recommended by Feng et al. [45]. The evaluation of measured data and the experimental arrangement followed the EN 10115-18 [46]. The water absorption coefficient was calculated using a one-tangent method [47], and the capillary moisture content w_{cap} ($\text{kg}\cdot\text{m}^{-3}$) was derived as the maximum of water imbibition curve obtained in a capillary absorption test. Usually, A_w is measured at (21 ± 2) °C. In our case, the laboratory temperature reached (25 ± 2) °C. Therefore, the temperature compensation of assessed A_w (25 °C) value was done as introduced in Equation (3):

$$A_w(21 \text{ }^\circ\text{C}) = \frac{A_w(T)}{0.0112(T - 273.15) + 0.7756} \quad (3)$$

where T (K) is the absolute temperature [45].

Based on the values of the water absorption coefficient A_w (21 °C) and capillary moisture content w_{cap} , the apparent moisture diffusivity D_{app} ($\text{m}^2\cdot\text{s}^{-1}$) was calculated using Equation (4) as originally proposed by Kumaran [48]:

$$D_{\text{app}} = \left(\frac{A_w(21 \text{ }^\circ\text{C})}{w_{\text{cap}}} \right)^2 \quad (4)$$

The expanded combined uncertainty of the capillary absorption test was 2.3% for A_w (21 °C), 1.8% for w_{cap} , and that of the apparent moisture diffusivity assessment was 3.5%.

Heat transport and storage were described with thermal conductivity λ ($\text{W}\cdot\text{m}^{-1}\cdot\text{K}^{-1}$), thermal diffusivity a ($\text{m}^2\cdot\text{s}^{-1}$), and volumetric heat capacity C_v ($\text{J}\cdot\text{m}^{-3}\cdot\text{K}^{-1}$) measurements, which were carried out by a transient plane source technique [49,50]. A TPS 1500 hot-disk thermal constant analyzer (Hot Disk AB, Göteborg, Sweden) with a Kapton-insulated sensor was used. Tests were conducted at room temperature (23 ± 2) °C. The dried specimens had dimension 40 mm \times 40 mm \times 70 mm. The sensor was placed between two parallel specimens, the cross-section of the specimens contact was 40 mm \times 40 mm (see Figure 4 for the measurement arrangement).



Figure 4. Experimental setup for thermophysical parameter measurement.

The durability of the developed lightweight composites in terms of water damage was evaluated using the water resistance coefficient [51] that was calculated using Equation (5):

$$\alpha_w = \frac{f_{c24w}}{f_c} \quad (5)$$

where f_{c24w} is the compressive strength of composites immersed in water for 24 h.

Optical microscopy of composite samples and lightweight aggregates was performed by a Navitar macro-optics (Rochester, NY, USA) microscope with optical zoom up to 110× and recorded with a Sony 2/3" digital camera having a resolution of 5 Mpixels. The sample was illuminated by a white LED ring light source with individually addressable segments and intensity. NIS-Elements BR 5.21.02 software (Prague, Czech Republic) with an extended depth of focus module (EDF) was used for imaging and analysis of the samples.

3. Results and Discussion

The specific density of used fillers ρ_{sf} is presented in Table 2. The highest density had silica sand which was in agreement with its dense and solid character. Both rubber and glass granulates had low specific densities due to their high porosity and the nature of their origin. For these materials, the effect of particle size was quite visible. Typically, the coarser granules yielded lower specific density. This feature was more distinct for Liaver particles rather than for the processed rubber.

Table 2. The specific density of applied aggregates.

Filler	Specific Density ρ_{sf} (kg·m ⁻³)
Silica Sand	2652
Granulated rubber	
0–1 mm	1195
1–2 mm	1172
Liaver	
0.1–0.3 mm	1240
0.25–0.5 mm	843
0.5–1.0 mm	717
1.0–2.0 mm	579

There are many types of lightweight aggregates with density ranging from $50 \text{ kg}\cdot\text{m}^{-3}$ (expanded perlite) to $1000 \text{ kg}\cdot\text{m}^{-3}$ (clinker) or even more [52]. These enable the production of construction composites with a wide range of properties meeting specific technical and functional requirements. The dry powder density of loose fillers and those compacted for 90 s is given in Table 3. For these materials, thermal parameters are also introduced.

Table 3. Powder density and thermal properties of aggregates.

Aggregate	State	Powder Density $\rho_p \text{ (kg}\cdot\text{m}^{-3}\text{)}$	Thermal Conductivity $\lambda_f \text{ (W}\cdot\text{m}^{-1}\cdot\text{K}^{-1}\text{)}$	Volumetric Heat Capacity $C_{wf} \times 10^6 \text{ (J m}^{-3}\cdot\text{K}^{-1}\text{)}$
Silica Sand	loose	1363	0.399	0.256
	compacted	1910	0.539	0.324
Granulated rubber	loose	441	0.085	0.270
	compacted	517	0.096	0.290
Liaver	loose	305	0.080	0.237
	compacted	346	0.094	0.249

The particle size distribution of silica sand, waste tire rubber, and Liaver is graphed in Figure 5. The mixture of Liaver granules gave similar grain size distribution to silica sand. Particles of rubber granulate were slightly coarser compared to two other tested aggregates, but their maximum size was identical.

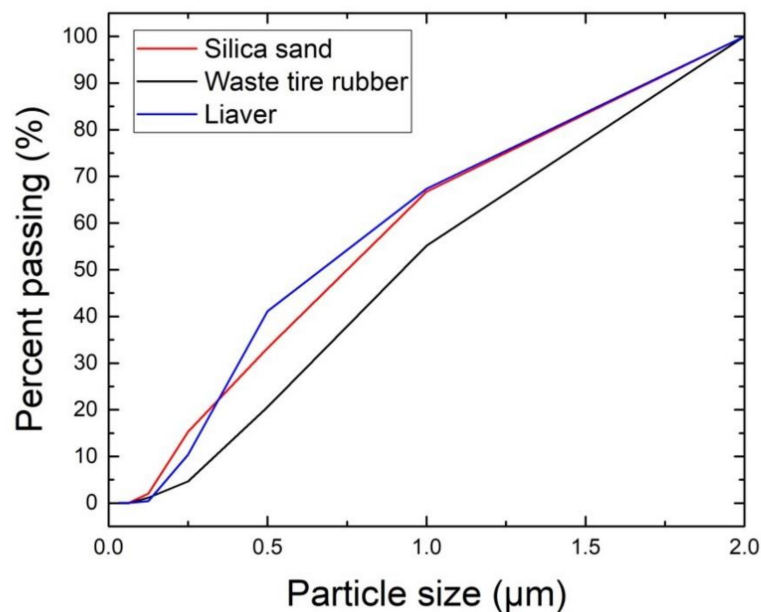


Figure 5. Particle size distribution of silica sand, waste tire rubber, and Liaver.

Macrostructural parameters of hardened composites are summarized in Table 4. The reference material MOC-S exhibited high dry bulk density, specific density and, thus, low porosity, which are typical for MOC-based materials [53]. The replacement of silica sand with processed rubber greatly decreased both the specific density and bulk density of rubberized composites which resulted in the increased porosity of these materials. Due to the lack of standards for MOC-based materials, we used standard EN 206-1 [54] for the classification of the developed materials, which covers structural lightweight concrete. Lightweight concrete must have an oven-dry density in the range $800\text{--}2000 \text{ kg}\cdot\text{m}^{-3}$, which is then divided into density classes with a span of $200 \text{ kg}\cdot\text{m}^{-3}$ [55]. In this respect, composites MOC-WT and MOC-WT+L10 were categorized into class LC 1.4, and materials MOC-WT+20, MOC-WT+30 into class LC 1.3, respectively.

Table 4. Workability of fresh mixtures and macrostructural parameters of hardened composites.

Materials	Spread Diameter (mm)	ρ_s (kg·m ⁻³)	ρ_b (kg·m ⁻³)	Ψ (%)
MOC-S	160/165 ± 5	2320 ± 28	2165 ± 30	6.7 ± 0.1
MOC-WT	125/125 ± 5	1671 ± 20	1440 ± 20	13.8 ± 0.3
MOC-WT+L10	130/130 ± 5	1662 ± 20	1413 ± 20	15.0 ± 0.3
MOC-WT+L20	130/135 ± 5	1654 ± 20	1365 ± 19	17.5 ± 0.4
MOC-WT+L30	135/135 ± 5	1609 ± 19	1316 ± 18	18.2 ± 0.4

In Table 4, the workability of fresh mixtures is characterized by the measured spread diameter. The flow diameter greatly dropped with the use of rubber granulate, which was assigned to its uniform particles size, shape, and their rugged surface. On the other hand, the use of Liaver improved slightly the workability of fresh mixtures compared to full substitution of silica sand with processed waste tires. This was due to oval-shaped and smooth granules of expanded glass.

The parameters that characterize the strength and stiffness of examined hardened composites are given in Table 5. The control material made of silica sand and MOC binder showed high mechanical strength and dynamic elastic modulus, which was in agreement with previously published papers [56,57]. One must take into account the high mechanical resistance which was obtained after 14 days of curing, and high flexural/compressive strength ratio that are superior properties of MOC binder to ordinary Portland cement [58].

Table 5. Mechanical parameters of hardened composites.

Materials	f_t (MPa)	f_c (MPa)	E_d (GPa)
MOC-S	18.9 ± 0.3	80.1 ± 1.1	44.5
MOC-WT	4.5 ± 0.1	12.7 ± 0.2	8.6
MOC-WT+L10	3.8 ± 0.1	11.4 ± 0.2	9.4
MOC-WT+L20	4.1 ± 0.1	11.7 ± 0.2	9.6
MOC-WT+L30	5.3 ± 0.1	11.9 ± 0.2	10.0

The sand substitution by lightweight aggregate resulted in a significant decrease in mechanical resistance. It was due to the lower powder density and specific density of both rubber and expanded glass granulates in comparison with silica sand. This finding was also in agreement with the porosity data, as the higher porosity brought lower mechanical strength and stiffness. As the density of Liaver was lower than that of shredded rubber, the compressive strength of composite MOC-WT was slightly higher compared to materials with Liaver addition. On the other hand, composites with expanded glass yielded higher modulus of elasticity, but the differences were typically small, similarly as observed for the flexural strength values. The minimum strength class of lightweight concrete given in the EN 206-1 [54] is LC8/9 that refers to a characteristic cylindrical compressive strength of 8 MPa and cubic strength of 9 MPa. This condition met all lightweight composites that nearly satisfied criteria of the strength class LC12/13 which is required by the design standard EN 1992-1-1 [59] for the structural lightweight concrete.

The parameters characterizing the water imbibition and storage in researched composites are shown in Table 6. These parameters are of the particular importance as MOC-based materials are generally considered as susceptible to moisture attack and damage [60]. The 24 h water absorption and both water transport parameters were very low, which pointed only to limited moisture ingress. In case of MOC-S, the rate of water imbibition was restricted by the low open porosity of this material. The limited moisture transport in lightweight composites was due to the non-absorbing and repellent character of rubber and glass granulates which surpassed the effect of higher porosity of these materials compared to that of the reference composite.

Table 6. Hygric parameters of hardened composites.

Materials	W_a (%)	A_w $\times 10^{-4}$ (kg·m ⁻² ·s ^{-1/2})	w_{cap} (kg·m ⁻³)	D_{app} $\times 10^{-9}$ (m ² ·s ⁻¹)
MOC-S	1.33 ± 0.02	6.0 ± 0.1	50.3 ± 0.9	0.14 ± 0.03
MOC-WT	2.01 ± 0.02	13.3 ± 0.3	63.5 ± 1.1	0.44 ± 0.10
MOC-WT+L10	2.45 ± 0.03	13.7 ± 0.3	74.7 ± 1.3	0.33 ± 0.08
MOC-WT+L20	2.51 ± 0.03	14.0 ± 0.3	75.5 ± 1.4	0.34 ± 0.08
MOC-WT+L30	2.86 ± 0.03	19.6 ± 0.5	79.7 ± 1.4	0.61 ± 0.14

The thermophysical properties of the investigated composites determined on dry samples using a hot disk apparatus are introduced in Table 7. Due to the low porosity of MOC-S its thermophysical parameters were high. The ability to transport and store heat was similar as that presented by Záleská et al. [61]. Here, it must be stated the thermal behavior of MOC-based materials was only rarely studied up to now, although numerous studies reported on their mechanical properties and precipitation of hydrated-like products within an MOC setting. The lightened composites exhibited decelerated heat transport and dropped heat storage, whereas the measured thermal parameters were results of the competition of two effects, namely of high porosity and thermal properties of lightweight fillers themselves. The use of Liaver slightly decreased the λ and C_v values in comparison with the composites with full replacement of silica sand by rubber granulate. This corresponded with the thermal parameters of both aggregates, and higher porosity of Liaver enriched materials.

Table 7. Thermophysical properties of hardened composites.

Materials	λ (W·m ⁻¹ ·K ⁻¹)	a $\times 10^{-6}$ (m ² ·s ⁻¹)	C_v $\times 10^6$ (J·m ⁻³ ·K ⁻¹)
MOC-S	3.247	1.455	2.233
MOC-WT	0.787	0.384	2.055
MOC-WT+L10	0.771	0.391	1.977
MOC-WT+L20	0.751	0.432	1.743
MOC-WT+L30	0.731	0.426	1.716

Figure 6 shows the control compressive strength and the compressive strength of composites placed for 24 h in water. The water resistance coefficient is introduced in Table 8. When being immersed for 24 h in water, the compressive strength of all investigated samples increased. This means the water immersion acted as an accelerating curing method. On a similar performance of MOC-based materials reported, Yu et al. [62] observed an increase in the mechanical resistance up to seven days of water exposure. On the other hand, authors observed that the compressive strength decreased with prolonged water immersion due to the decomposition of the main precipitated products [63,64].

The photographs of hardened samples provided by optical microscopy are presented in Figure 7. The dense structure of reference composite MOC-S is particularly visible. In lightweight composites, the incorporation and distribution of rubber and Liaver granules in the MOC matrix was observed.

Table 8. The water resistance coefficient.

Materials	α_w (GPa)
MOC-S	1.1
MOC-WT	1.2
MOC-WT+L10	1.3
MOC-WT+L20	1.2
MOC-WT+L30	1.2

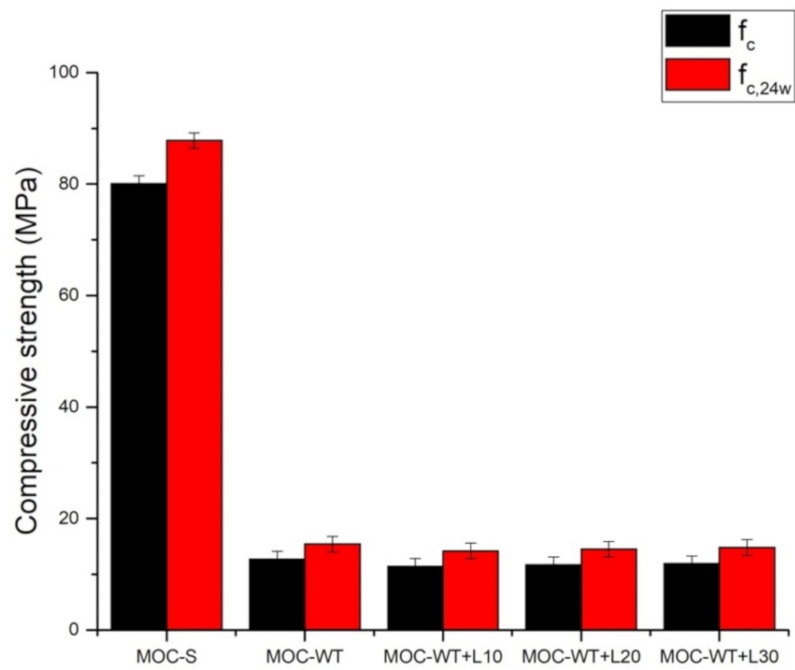


Figure 6. Comparison of the control compressive strength and that of samples exposed to water.

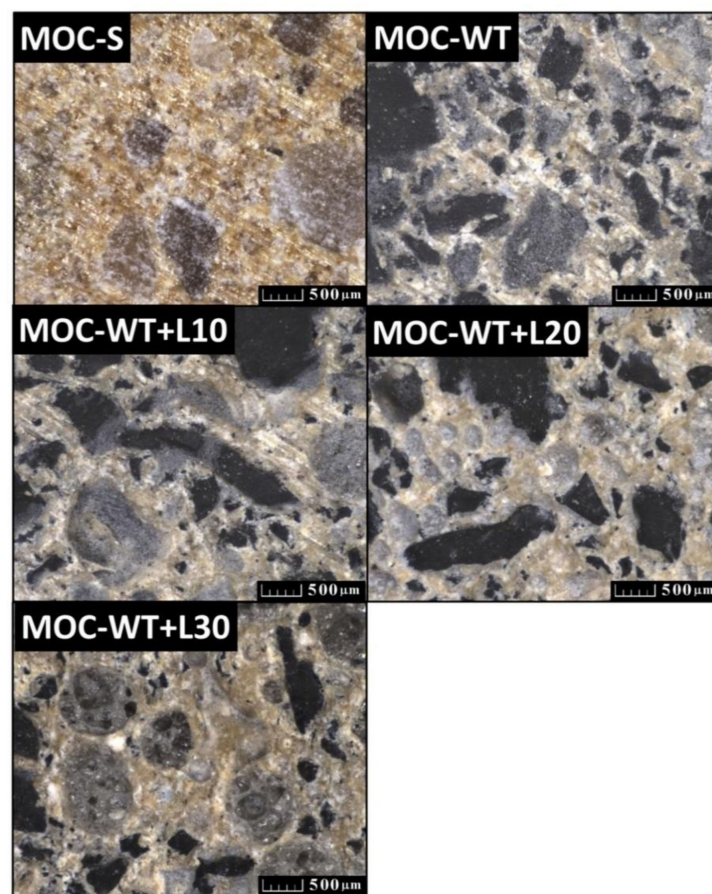


Figure 7. Photographs of composites acquired by optical microscopy (scale bar: 500 μ m).

4. Conclusions

Novel lightweight composites for construction use were developed and tested. The materials were made of MOC and processed waste tires which were partially substituted with granulate of expanded glass. The use of a lightweight filler produced from waste tires can help to reduce the continuously-increasing amount of this type of waste and, thus, increase the sustainability of the construction industry. Moreover, as MOC is considered to be a low-carbon binder, the manufactured composites represent an eco-efficient alternative to Portland cement-based materials whose production enormously depletes natural resources and contributes substantially to the generation and emission of greenhouse gases. The use of processed waste also brings financial benefits. Based on the obtained experimental data, the following findings were highlighted:

- (i) application of processed ELT and glass granulate resulted in an increased porosity and great drop in bulk density;
- (ii) the developed lightweight materials had sufficient mechanical strength and stiffness which were suitable also for structural applications;
- (iii) the use of non-absorbing rubber particles and glass granulate repelled the water ingress, the composites, therefore, exhibited low permeability for water;
- (iv) the both lightweight aggregates used improved the thermal insulation performance of the manufactured composites compared to reference material with silica sand as the only filler;
- (v) because of the low water penetration, the novel materials were durable with respect to moisture damage.

Summarizing the results of the conducted tests and analyses, the rubberized MOC-based composites may represent a basis for modern construction materials with improved durability and thermal insulation performance. These composites thus represent an interesting alternative to traditional building products.

Author Contributions: Conceptualization: M.P. and Z.P.; methodology: M.P., O.J., and Z.P.; investigation: M.P., A.P., M.Z., O.J., and P.R.; data curation: M.P., O.J., and Z.P., writing—original draft preparation: M.P. and Z.P.; supervision: M.P., O.J., and Z.P.; project administration: M.P. and O.J. All authors have read and agreed to the published version of the manuscript.

Funding: This research was funded by the Czech Science Foundation, grant number 19-00262S—Reactive magnesia cements-based composites with selected admixtures and additives.

Conflicts of Interest: The authors declare no conflict of interest.

References

1. Eriksson, O.; Bisailon, M.; Haraldsson, M.; Sundberg, J. Integrated waste management as a mean to promote renewable energy. *Renew. Energy* **2017**, *61*, 38–42.
2. Byström, J. Eco efficiency, a path towards integrated resource management. *Waste Manag.* **2012**, *32*, 797–798.
3. ETRMA—European Tyre & Rubber Manufacturers' Association. European Tyre and Rubber Industry Statistics. 2019. Available online: <https://www.etrma.org/wp-content/uploads/2019/10/20191114-Statistics-booklet-2019-Final-for-web.pdf> (accessed on 15 September 2020).
4. Sienkiewicz, M.; Kucinska-Lipka, J.; Janik, H.; Balas, A. Progress in used tyres management in the European Union: A review. *Waste Manag.* **2012**, *32*, 1742–1751. [[CrossRef](#)] [[PubMed](#)]
5. Toretta, V.; Rada, E.C.; Ragazzi, M.; Trulli, E.; Istrate, I.A.; Cioca, L.I. Treatment and disposal of tyres: Two EU approaches. A review. *Waste Manag.* **2015**, *45*, 152–160. [[CrossRef](#)] [[PubMed](#)]
6. Noorzad, R.; Raveshi, M. Mechanical behavior of waste tire crumbs-sand mixtures determined by triaxial tests. *Geotech. Geol. Eng.* **2017**, *35*, 1793–1802.
7. Pantea, D.; Darmstadt, H.; Kaliaguine, S.; Roy, C. Heat-treatment of carbon blacks obtained by pyrolysis of used tires. Effect on the surface chemistry, porosity and electrical conductivity. *J. Anal. Pyrol.* **2003**, *67*, 55–76. [[CrossRef](#)]

8. Moreno-Navarro, F.; Sol-Sánchez, M.; Rubio-Gámez, M.C. Reuse of deconstructed tires as anti-reflective cracking mat systems in asphalt pavements. *Constr. Build. Mater.* **2014**, *53*, 182–189. [[CrossRef](#)]
9. Xiao, F.; Amirkhanian, S.N. Laboratory investigation of moisture damage in rubberised asphalt mixtures containing reclaimed asphalt pavement. *Int. J. Pavement Eng.* **2009**, *10*, 319–328.
10. Yu, X.; Wang, Y.; Luo, Y. Effects of types and content of warm-mix additives on CRMA. *J. Mater. Civ. Eng.* **2013**, *25*, 939–945.
11. Shu, X.; Huang, B. Recycling of waste tire rubber in asphalt and portland cement concrete: An overview. *Constr. Build. Mater.* **2014**, *67*, 217–224.
12. Akisetty, C.; Xiao, F.; Gandhi, T.; Amirkhanian, S. Estimating correlations between rheological and engineering properties of rubberized asphalt concrete mixtures containing warm mix asphalt additive. *Constr. Build. Mater.* **2011**, *25*, 950–956. [[CrossRef](#)]
13. Lo Presti, D.; Airey, G. Tyre rubber-modified bitumens development: The effect of varying processing conditions. *Road Mater. Pavement* **2013**, *14*, 888–900. [[CrossRef](#)]
14. Gupta, T.; Chaudhary, S.; Sharma, R.K. Assessment of mechanical and durability properties of concrete containing waste rubber tire as fine aggregate. *Constr. Build. Mater.* **2014**, *73*, 562–574. [[CrossRef](#)]
15. Siddique, R.; Naik, T.R. Properties of concrete containing scrap-tire rubber—An overview. *Waste Manag.* **2004**, *24*, 563–569. [[CrossRef](#)] [[PubMed](#)]
16. Liu, H.; Wang, X.; Jiao, Y.; Sha, T. Experimental investigation of the mechanical and durability properties of crumb rubber concrete. *Materials* **2019**, *9*, 172. [[CrossRef](#)]
17. Boudaoud, Z.; Beddar, M. Effects of recycled tires rubber aggregates on the characteristics of cement concrete. *Open J. Civ. Eng.* **2012**, *2*, 193–197. [[CrossRef](#)]
18. Záleská, M.; Pavlík, Z.; Čítek, D.; Jankovský, O.; Pavlíková, M. Ecco-friendly concrete with scrap-tyre-rubber-based aggregate – Properties and thermal stability. *Constr. Build. Mater.* **2019**, *225*, 709–722. [[CrossRef](#)]
19. Lavagna, L.; Nisticò, R.; Sarasso, M.; Pavese, M. An analytical mini-review on the compression strength of rubberized concrete as a function of the amount of recycled tires crumb rubber. *Materials* **2020**, *13*, 1234. [[CrossRef](#)] [[PubMed](#)]
20. Mohammed, B.S.; Hossain, K.M.A.; Swee, J.T.E.; Wong, G.; Abdullahi, M. Properties of crumb rubber hollow concrete block. *J. Clean. Prod.* **2012**, *23*, 57–67. [[CrossRef](#)]
21. Sukontasukkul, P. Use of crumb rubber to improve thermal and sound properties of pre-cast concrete panel. *Constr. Build. Mater.* **2008**, *23*, 1084–1092. [[CrossRef](#)]
22. de Souza Kazmierczak, C.; Schneider, S.D.; Aguilera, O.; Albert, C.C.; Mancio, M. Rendering mortars with crumb rubber: Mechanical strength, thermal and fire properties and durability behavior. *Constr. Build. Mater.* **2020**, *253*, 119002. [[CrossRef](#)]
23. Oikonomou, N.; Mavridou, S. Improvement of chloride ion penetration resistance in cement mortars modified with rubber from worn automobile tires. *Cem. Concr. Compos.* **2009**, *31*, 403–407. [[CrossRef](#)]
24. Benazzouk, A.; Douzane, O.; Langlet, T.; Mezreb, K.; Roucoult, J.M.; Quéneudec, M. Physico-mechanical properties and water absorption of cement composite containing shredded rubber wastes. *Cem. Concr. Compos.* **2007**, *29*, 732–740. [[CrossRef](#)]
25. Xu, H.; Lian, J.; Gao, M.; Fu, D.; Yan, Y. Self-Healing Concrete Using Rubber Particles to Immobilize Bacterial Spores. *Materials* **2019**, *12*, 2313. [[CrossRef](#)] [[PubMed](#)]
26. Segre, N.; Joekes, I.; Galves, A.D.; Rodrigues, J.A. Rubber-mortar composite: Effect of composition on properties. *J. Mater. Sci.* **2004**, *39*, 3319–3327. [[CrossRef](#)]
27. Záleská, M.; Pavlíková, M.; Jankovský, O.; Lojka, M.; Pivák, A.; Pavlík, Z. Experimental Analysis of MOC Composite with a Waste-Expanded Polypropylene-Based Aggregate. *Materials* **2018**, *11*, 931. [[CrossRef](#)]
28. Li, Y.; Yu, H.; Zheng, L.; Wen, J.; Wu, C.; Tan, Y. Compressive strength of fly ash magnesium oxychloride cement containing granite wastes. *Constr. Build. Mater.* **2013**, *38*, 1–7. [[CrossRef](#)]
29. Jankovský, O.; Lojka, M.; Lauermannová, A.-M.; Antončík, F.; Pavlíková, M.; Záleská, M.; Pavlík, Z.; Pivák, A.; Sedmidubský, D. Towards novel building materials: High-strength nanocomposites based on graphene, graphite oxide and magnesium oxychloride. *Appl. Mater. Today* **2020**, *20*, 100766. [[CrossRef](#)]
30. Qing, H.; Ying, L.; Jing, W.; Weixin, Z.; Chenggong, C.; Jinmei, D.; Danchun, A.; Xueming, X.; Yuan, Z. Effect of ethyl silicate on the water resistance of magnesium oxychloride cement. *Ceram. Silikáty* **2020**, *64*, 75–83. [[CrossRef](#)]

31. Deng, D. The mechanism for soluble phosphates to improve the water resistance of magnesium oxychloride cement. *Cem. Concr. Res.* **2008**, *33*, 1311–1317. [[CrossRef](#)]
32. Bockstal, L.; Berchem, T.; Schmetz, Q.; Richel, A. Devulcanisation and reclaiming of tires and rubber by physical and chemical processes: A review. *J. Clean. Prod.* **2019**, *236*, 117574.
33. Záleská, M.; Pavlíková, M.; Pokorný, J.; Jankovský, O.; Pavlík, Z.; Černý, R. Structural, mechanical and hygrothermal properties of lightweight concrete based on the application of waste plastics. *Constr. Build. Mater.* **2018**, *180*, 1–11.
34. *Testing for Geometrical Properties of Aggregates—Part 1: Determination of Particle Size Distribution, EN 933-1*; European Committee for Standardization: Brussels, Belgium, 2012.
35. *Binders for Magnesite Screeds—Caustic Magnesia and Magnesium Chloride—Part 2: Test Methods, EN 14016-2*; European Committee for Standardization: Brussels, Belgium, 2004.
36. Pivák, A.; Pavlíková, M.; Záleská, M.; Lojka, M.; Jankovský, O.; Pavlík, Z. Magnesium oxychloride cement composites with silica filler and coal fly ash admixture. *Materials* **2020**, *13*, 2537.
37. *Methods of Test for Mortar for Masonry—Part 10: Determination of Dry Bulk Density of Hardened Mortar, EN 1015-10*; European Committee for Standardization: Brussels, Belgium, 1999.
38. *Methods of Test for Mortar for Masonry—Part 11: Determination of Flexural and Compressive Strength of Hardened Mortar, EN 1015-11*; European Committee for Standardization: Brussels, Belgium, 1999.
39. Malhotra, V.M.; Carino, N.J. *Handbook on Nondestructive Testing of Concrete*, 2nd ed.; CRC Press LLC: Boca Raton, FL, USA, 2003.
40. He, P.; Poon, C.S.; Tsang, D.C.W. Effect of pulverized fuel ash and CO₂ curing on the water resistance of magnesium oxychloride cement (MOC). *Cem. Concr. Res.* **2017**, *97*, 115–122.
41. Tang, S.; Hu, Y.; Ren, W.; Yu, P.; Huang, Q.; Qi, X.; Li, Y.; Chen, E. Modeling on the hydration and leaching of eco-friendly magnesium oxychloride cement paste at the micro-scale. *Constr. Build. Mater.* **2019**, *204*, 684–690.
42. Zhou, J.; Liu, P.; Wu, C.; Du, Z.; Zong, J.; Miao, M.; Pang, R.; Yu, H. Properties of foam concrete prepared from magnesium oxychloride cement. *Ceram. Silikáty* **2020**, *64*, 200–214.
43. *Natural Stone Test Methods—Determination of Water Absorption at Atmospheric Pressure, EN 13755*; European Committee for Standardization: Brussels, Belgium, 2008.
44. Pavlík, Z.; Černý, R. Determination of moisture diffusivity as a function of both moisture and temperature. *Int. J. Thermophys.* **2012**, *33*, 1704–1714.
45. Feng, C.; Guimarães, A.S.; Ramos, N.; Sun, L.; Gawin, D.; Konca, P.; Hall, C.; Zhao, J.; Hirsch, H.; Grunewald, J.; et al. Hygric properties of porous building materials (VI): A round robin campaign. *Build. Environ.* **2020**, *185*, 107242.
46. *Methods of Test for Mortar for Masonry—Part 18: Determination of Water-Absorption Coefficient Due to Capillary Action of Hardened Mortar, EN 1015-18*; European Committee for Standardization: Brussels, Belgium, 2002.
47. Feng, C.; Janssen, H. Hygric properties of porous building materials (III): Impact factors and data processing methods of the capillary absorption test. *Build. Environ.* **2018**, *134*, 21–34.
48. Kumaran, M.K. Moisture diffusivity of building materials from water absorption measurements. *J. Therm. Envel. Build. Sci.* **1999**, *22*, 349–355.
49. Gustafsson, S.E. Transient plane source techniques for thermal conductivity and thermal diffusivity measurements of solid materials. *Rev. Sci. Instrum.* **1991**, *62*, 797. [[CrossRef](#)]
50. Sizov, A.D.; Cederkrantz, D.; Salmi, L.; Rosén, A.; Jacobson, L.S.; Gustafsson, S.E.; Gustavsson, M. Thermal conductivity versus depth profiling of inhomogeneous materials using the hot disc technique. *Rev. Sci. Instrum.* **2016**, *87*, 074901. [[CrossRef](#)]
51. Xu, B.; Ma, H.; Hu, C.; Li, Z. Influence of cenospheres on properties of magnesium oxychloride cement-based composites. *Mater. Struct.* **2016**, *49*, 1319–1326.
52. Chandra, S.; Berntsson, L. *Lightweight Aggregate Concrete, Science, Technology, and Applications*; Noyes Publications/Wiliam Andrew Publishing: Norwich, CT, USA, 2002.
53. Pivák, A.; Pavlíková, M.; Záleská, M.; Lojka, M.; Lauermannová, A.-M.; Jankovský, O.; Pavlík, Z. Low-carbon composite based on MOC, silica sand and ground porcelain insulator waste. *Processes* **2020**, *8*, 829. [[CrossRef](#)]
54. *Concrete—Specification, Performance, Production and Conformit, EN 206+A1*; European Committee for Standardization: Brussels, Belgium, 2016.
55. Thienel, K.-C.; Haller, T.; Beuntner, N. Lightweight concrete—From basics to innovations. *Materials* **2020**, *13*, 1120. [[CrossRef](#)] [[PubMed](#)]

56. Guo, Y.; Zhang, Y.; Soe, K.; Hutchinson, W.D.; Timmers, H.; Poblete, M.R. Effect of fly ash on mechanical properties of magnesium cement under water attack. *Struct. Concr.* **2020**, *21*, 1181–1199. [[CrossRef](#)]
57. Hall, D.A.; Stevens, R.; El-Jazairi, B. The effect of retarders on the microstructure and mechanical properties of magnesia–phosphate cement mortar. *Cem. Concr. Res.* **2001**, *31*, 455–465.
58. Misra, A.K.; Mathur, R. Magnesium oxychloride cement concrete. *Bull. Mat. Sci.* **2007**, *30*, 239–246. [[CrossRef](#)]
59. *Eurocode 2: Design of Concrete Structures. Part 1-1, General Rules and Rules for Buildings, EN 1992-1-1*; European Committee for Standardization: Brussels, Belgium, 2019.
60. Guo, Y.; Zhang, Y.; Soe, K.; Pulham, M. Recent development in magnesium oxychloride cement. *Struct. Concr.* **2018**, *19*, 1290–1300. [[CrossRef](#)]
61. Záleská, M.; Pavlíková, M.; Jankovský, O.; Lojka, M.; Antončík, F.; Pivák, A.; Pavlík, Z. Influence of waste plastic aggregate and water-repellent additive on the properties of lightweight magnesium oxychloride cement composite. *Appl. Sci.* **2019**, *9*, 5463. [[CrossRef](#)]
62. Yu, K.; Guo, Y.; Zhang, Y.X.; Soe, K. Magnesium oxychloride cement-based strain-hardening cementitious composite: Mechanical property and water resistance. *Constr. Build. Mater.* **2020**, *261*, 119970. [[CrossRef](#)]
63. Tan, Y.; Liu, Y.; Grover, L. Effect of phosphoric acid on the properties of magnesium oxychloride cement as biomaterial. *Cem. Concr. Res.* **2014**, *56*, 69–74. [[CrossRef](#)]
64. Li, Y.; Yu, H. Rapid assessment method for water resistance of magnesium oxychloride cement based on measurement of high temperature erosion thickness. *J. Chin. Ceram. Soc.* **2014**, *42*, 1047–1054.

Publisher’s Note: MDPI stays neutral with regard to jurisdictional claims in published maps and institutional affiliations.



© 2020 by the authors. Licensee MDPI, Basel, Switzerland. This article is an open access article distributed under the terms and conditions of the Creative Commons Attribution (CC BY) license (<http://creativecommons.org/licenses/by/4.0/>).